UNIVERSITY OF CAMBRIDGE
DEPARTMENT OF ENGINEERING

Part IIA Easter Project 2021 Final Individual Report

SA1: Aircraft Wing Analysis

Cody Lau (CHYL2)
Girton College

Contents

1. Summary

A Matlab code has been written over a 3-week period, using panel methods to model the lift and drag characteristics of aerofoil shapes as well as the boundary layer conditions. 2 aerofoils have been designed using this code, for low and high Reynold's numbers respectively. Each design involved a design process with multiple iterations to find the optimum lift-to-drag ratio, whilst also considering aerofoil usability and validity, such as stall characteristics. The accuracy and reliability of our Matlab numerical model have been evaluated, by first choosing a resolution to be used and comparing our results to real-world experimental data on known aerofoil geometries, as well as confirming justifications for assumptions in our model.

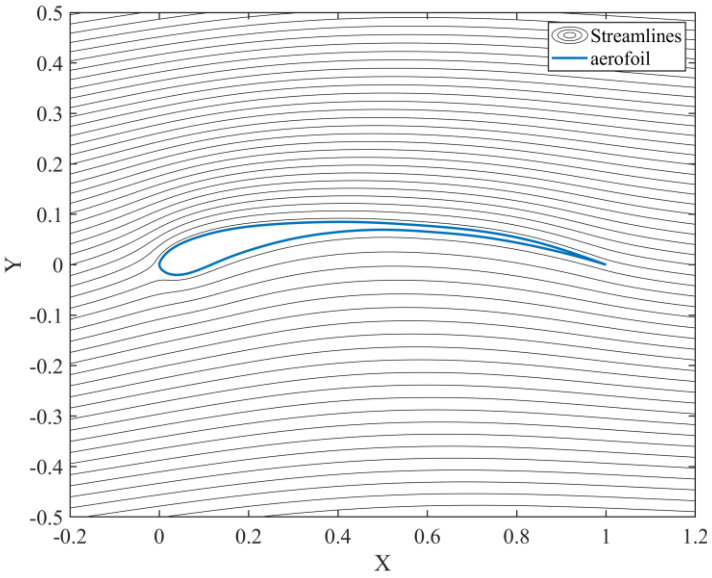

Figure 1a: Streamlines of low-Re design at design incidence (2.6°)

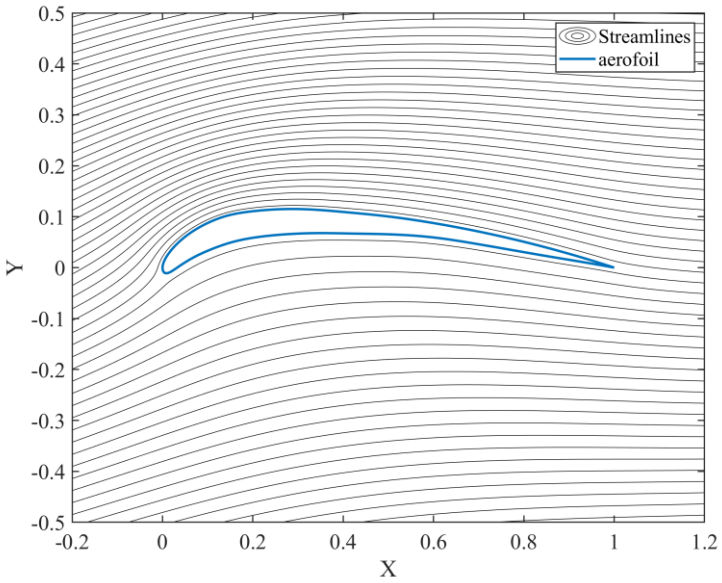

Figure 1b: Streamlines of high-Re design at optimum incidence (7.2°)

[Streamlines were plotted with an edited Matlab script from exercise 4, week 1]

2. Introduction

With today's high-performance computers being readily available, wing design approaches and processes have radically changed within the aerospace industry. In the past, optimisation of aerofoil shapes relied heavily on wind tunnel testing, which was expensive and time consuming. However, now most initial section designs are first evaluated through numerical calculations, with wind tunnel testing being used on the most optimum section designs. This allows a greater range of complex geometries and parameters to be developed.

This project aims: to carry out this numerical design process for two-dimensional aerofoil sections, to write a Matlab code for both the potential flow panel method and an integral boundary layer equation solver, and to produce an aerofoil analysis code which provides performance metrics such as life and drag. The second half of the project's objectives are to design 2 2D aerofoil sections and to optimise them for both low Reynold's Number (Re) and high Re using the written Matlab code. Great care will be taken to evaluate the strengths and

weaknesses of our written CFD code, as well as the role of the boundary layer in the overall aerofoil performance.

3. Numerical Model

3.1 Resolution Study

For our panel method code, the discretisation level must be found to optimise the runtime/computational power required while still achieving satisfactory accuracy. However, we must first reconsider the Kutta condition in our code. The trailing-edge surface velocity for both upper and lower surface is found by linear extrapolation, the actual trailing-edge velocity is then calculated by taking the average of the upper and lower surface trailing-edge velocity. The magnitudes of the velocities are equivalent to the vortex sheet strengths and these are linked to the pressure distribution with the use of Bernoulli's equation.

This new Kutta condition removes two unwanted effects in the computed pressure distribution. Firstly, a small 'wiggle' in the final three points which does not improve as the resolution is improved. Secondly, an extreme adverse pressure gradient within the final panel which leads to inaccuracies with the boundary layer calculations. The reason for the latter, is that the actual stagnation point at the trailing-edge lies within the boundary layer, meaning it is correlated to viscous effects. Therefore, imposing it on the inviscid, external solution is incorrect.

By comparing the exact pressure distribution with various number of panels, it was found that a resolution of 400 panels was sufficiently accurate and had no significant numerical errors. *Figure 3* shows that numerical errors were significant for 100 and 200-panels on a thin foil around the leading edge. Similarly, on a thick foil, only 100-panels shows significant deviation from the exact solution at the leading edge. *Figure 5* shows that downstream of the leading edge, the errors from the exact solution are negligible (0.035% for 400/800-panels). Therefore, for the rest of the design process, a resolution of 500-panels was chosen, and 800-panels was used for the final iterations of our design as it was noticed that the increased resolution had no significant increase in the runtime of our code.

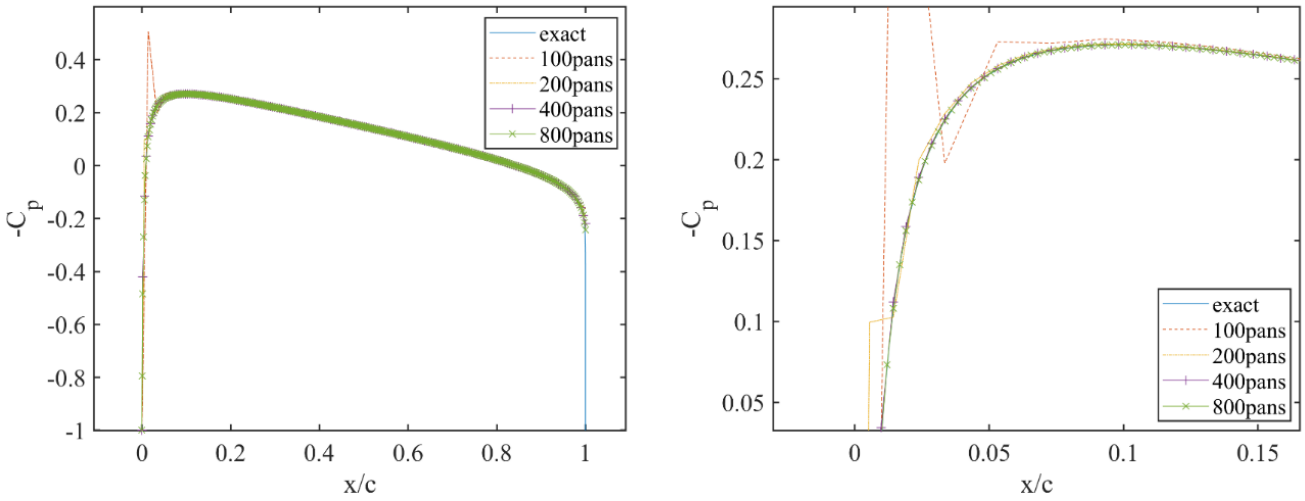

Figure 3: Pressure coefficient distribution for different resolutions on a thin aerofoil, zoomed in near leading edge for right figure

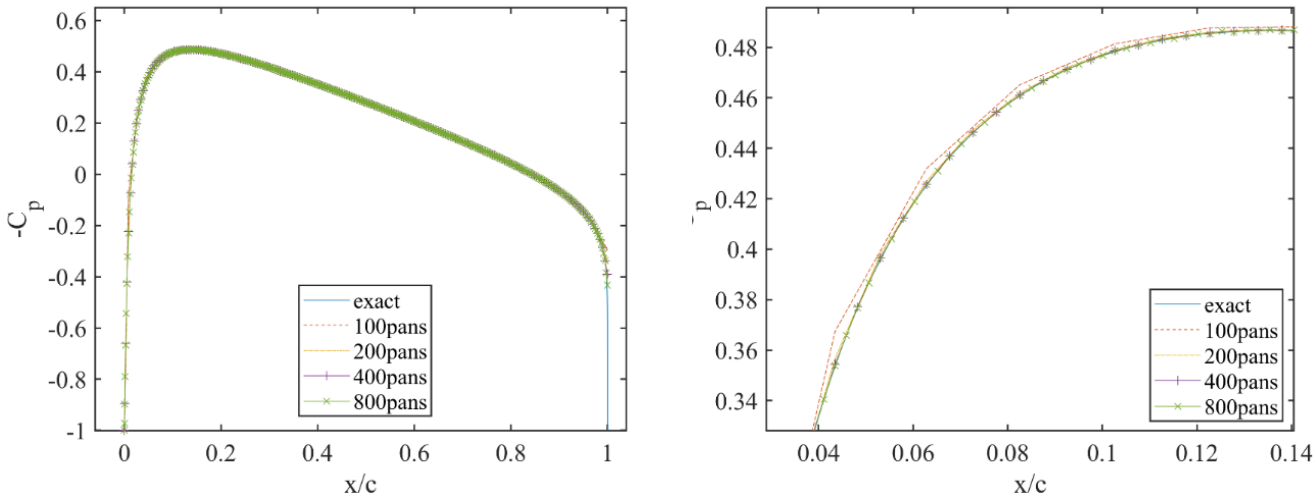

Figure 4: Pressure coefficient distribution for different resolutions on a thick aerofoil, zoomed in near leading edge for right figure

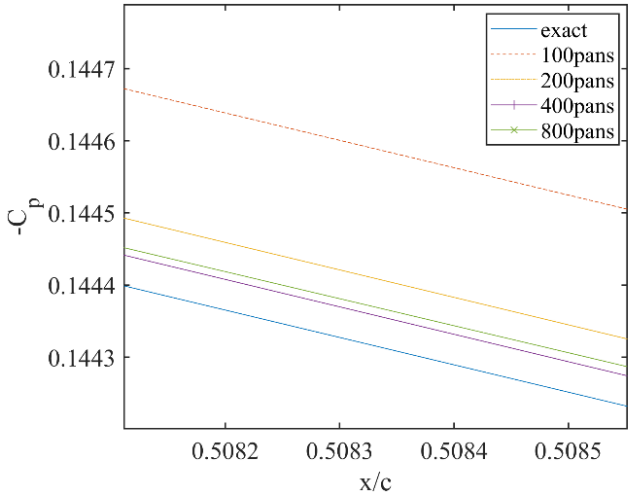

Figure 5: Zoomed pressure coefficient plot behind leading edge of a thin aerofoil

3.2 Boundary layer validation

The boundary layer code written in week 2 has been rewritten as a subroutine which returns the location of boundary layer state changes, and an array of displacement and momentum thickness given an input of x locations and the corresponding pressure coefficients. Previously i=1 was the start of the boundary layer but now it starts at zero.

To validate that the boundary layer code is correct, our laminar solution (Thwaites) is compared with Blasius's solution, and our turbulent solution with the power-law approximation for the turbulent section. As can be seen in *Figure 6*, both our solution match with what is expected closely. The separation locations found through this new subroutine also matches what was found in the week 2 exercises.

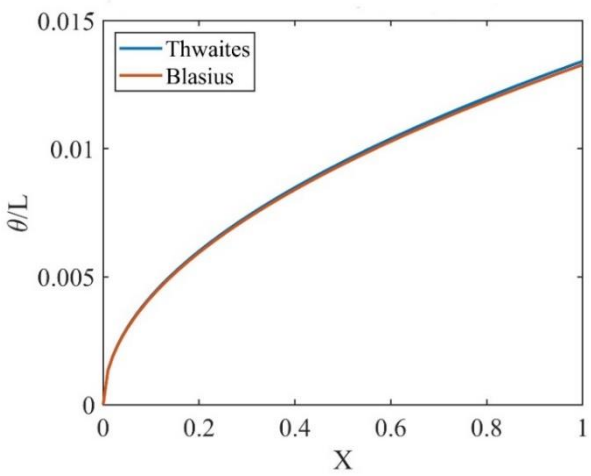

Figure 6a: Laminar momentum thickness growth

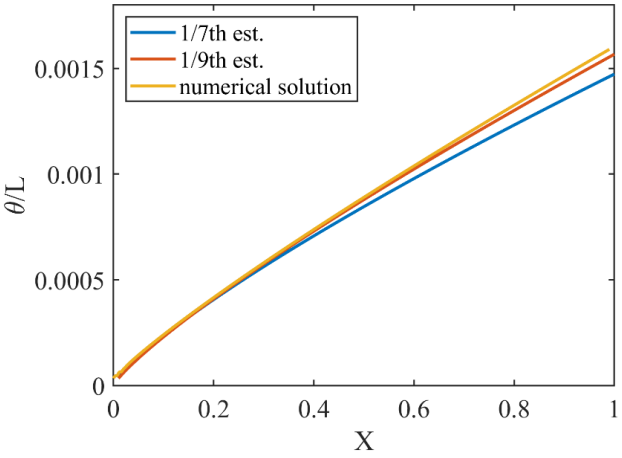

Figure 6b: Turbulent momentum thickness growth

3.3 Aerofoil Validation

To fully test our Matlab code before starting our main design process, one must validate it using an existing section geometry and compare our numerical results with its real-world experimental data. The aerofoils NACA-0012 and NACA-4412 were tested at Re = 3e6.

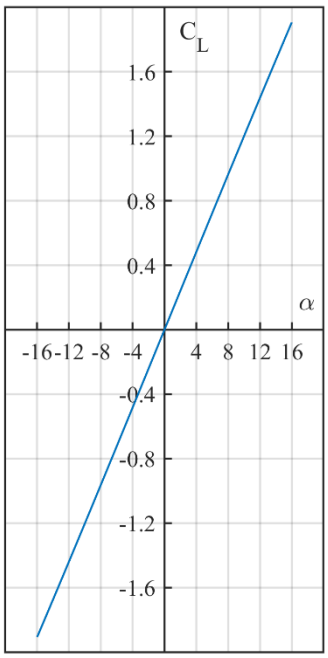

Figure 7a: Numerical angle of incidence against lift

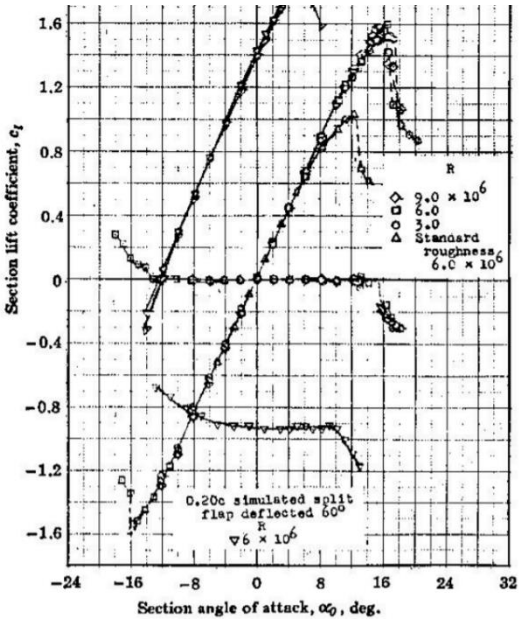

Figure 7b: Experimental angle of incidence against lift

Our results confirm that our code indeed outputs the correct performance metrics. For NACA-0012, our computational results for coefficient of lift (C_L) against angle of attack matches the experimental data very closely, only differing by 5.5% at 8° (*Figure 7*). Past 12° however, experimental data shows that the aerofoil is approaching stall where there is a slight decrease in gradient, and with full stall occurring at 16° where C_L drops abruptly. Our model for the lift does not consider stall, as C_L was calculated as $C_L = -2\frac{\Gamma}{Uc}$, where Γ is the total circulation which is calculated from the pressure distribution. This does not take into account the boundary

layer state, i.e. turbulent separation, where the shear stress at the aerofoil surface is zero. We can however, show that our code outputs turbulent separation on the upper surface at 15° at $x = 0.473c$, an indication that our model predicts stall accurately. Therefore, results for lift past the point of stall should be considered invalid.

Similarly, the C_D against C_L curve only shows a 6.6% difference in C_D between our numerical results and experimental data at $C_L = 1.2$ which is sufficiently close enough as there will always be some errors between theory and practice. Our results included points past $C_L = 1.2$ and are much higher around this region because as explained earlier our code for lift does not consider stall, whereas for experimental data results are invalid or do not exist at high angles.

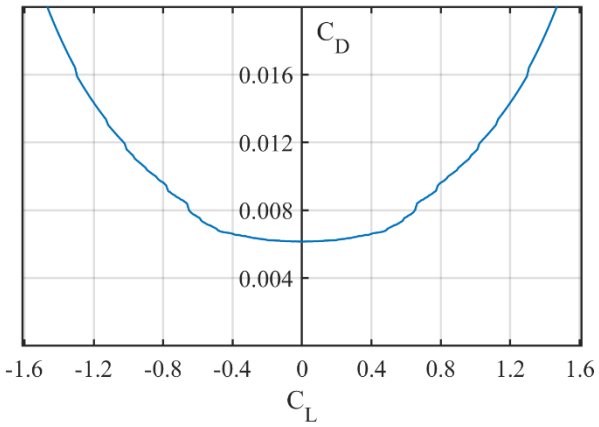

Figure 6a: Numerical lift against drag

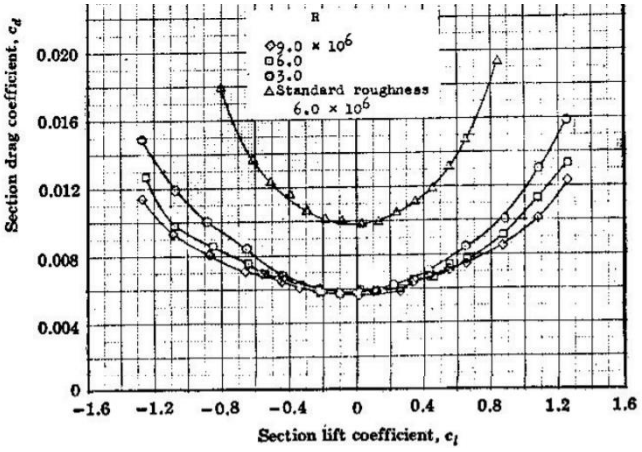

Figure 6b: Experimental lift against drag

The NACA-4412 aerofoil was also tested with our code and achieved very similar results to experimental data. A similar issue occurs around the stalling angles, and great care needs to be taken during the design process to consider where our code indicates stall through the location of turbulent separation on the upper surface.

The reliability of our model and results are discussed in greater detail in ***6. Reliability of Results.***

4. Aerofoil Design

The design process for both low and high Re will focus on optimising the lift-to-drag (L/D) ratio. This is explained in the *Breguet range equation:*

$$Range = \frac{U}{g}\frac{L/D}{sfc} log\left(\frac{Wstart}{Wend}\right)$$

Where given a fixed flight speed, specific fuel consumption and starting/end weight, the range in which an aircraft could fly to varies linearly with only L/D.

4.1 Design Process for Low Re Aerofoil (0.5×10^6)

For operating at low Re, we aim to create a 'Laminar Aerofoil', which is where a laminar boundary layer is maintained for as long as possible. This leads to reductions in drag compared to non-laminar aerofoils. This is because a laminar boundary layer exhibits slower growth, leading to a smaller wake size downstream of the trailing edge. Not to mention a drop in skin

friction drag. However, great care needs to be taken to avoid laminar separation near the leading edge, as explained earlier, our model does not predict behaviour post separation accurately.

Starting Aerofoil

To choose a starting aerofoil, we first look at aerofoils designed for laminar flow which is our main aim, such as NACA 6-series aerofoils [5]. Sources also mention that sections with concave afterbody contour (e.g. NACA 63 and 64 series) have the highest lift-curve slopes [4]. NACA 64-008A has a maximum thickness of 8% at 40% chord and no chamber. This aerofoil was chosen as it has the maximum thickness at a location most downstream out of all 6-series aerofoils. This location corresponds to the minimum pressure point and usually where the transition to turbulent occurs. This is because the pressure gradient becomes adverse downstream of the minimum pressure point. Having this point further back helps delays transition and maintains laminar flow for longer, reducing drag.

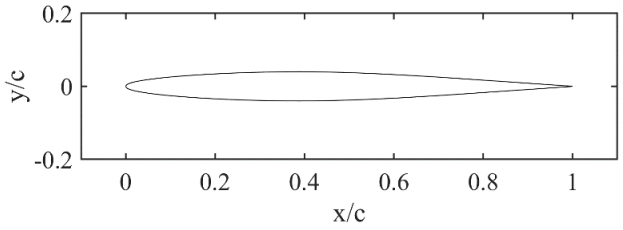

Figure 7a: Geometry of NACA 64-008A

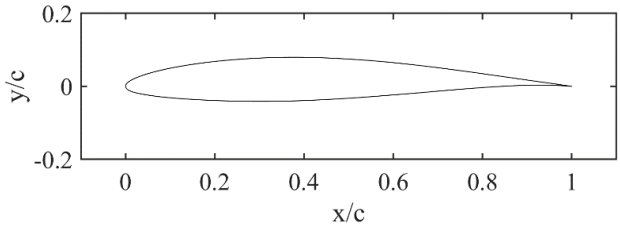

Figure 7b: Geometry of NACA 63-412

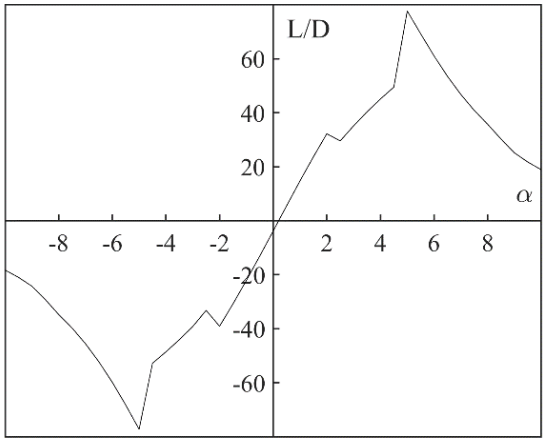

Figure 7c: Angle against lift-to -drag for NACA 64-008A

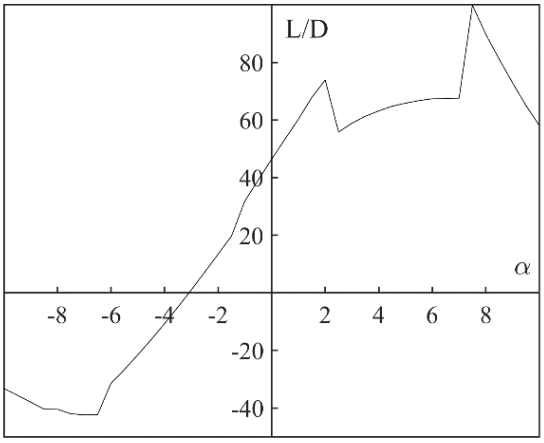

Figure 7d: Angle against lift-to-drag for NACA 63-412

The maximum L/D obtained for NACA 64-008A was 49.5 at an angle of attack of 4.5°. At angles greater than 4.5°, flow separation occurs on the upper surface. Our model does not predict behaviours beyond separation accurately, so results at these greater angles are invalid and not considered. A maximum L/D of 49.5 is low even for a starting aerofoil, so a different section was tested, the NACA 63-412. This section has a maximum thickness of 12% at 34.9% of chord, and a maximum camber of 2.2% at 50% chord.

This aerofoil is thicker, meaning drag would be expected to increase. Drag would also be higher due to the maximum thickness location being closer to the leading edge, so less laminar flow is maintained. However, we expect that the higher drag would be outweighed by the increase in lift due to camber, to give us an overall increase in maximum L/D. This was proven to be correct, with a maximum L/D of 73.89 at 2°, and a more advantageous stalling (upper surface separation) angle of 7°. Therefore, NACA 63-412 is chosen as our starting aerofoil.

First iteration – minimum pressure point

The aim of the first iteration is to bring the minimum pressure point towards the trailing edge, thus maintaining laminar flow for as long as possible, and reducing the drag. To achieve this the maximum thickness of the section is shifted towards the trailing edge.

Table 1: Results of starting aerofoil and first iteration for low-Re

			Upper		Lower	
Section	Max. L/D	α at max L/D	Laminar Separation	Turbulent Reattachment	Laminar Separation	Turbulent Reattachment
NACA-63412	73.89	2°	0.469c	0.492c	0.602c	0.603c
First iteration	97.42	2.5°	0.654c	0.684c	0.804c	0.840c

Both surfaces' gradients were made as smooth as possible, to avoid significant local adverse pressure gradients as they may lead to earlier separation/transition. Our results show that laminar flow was obtained over 65% of the upper surface and 80% of the lower surface, a large increase for both compared to the starting aerofoil. This led to a large reduction in the drag and as a result the maximum L/D was increased by a massive 31.8% to 97.42 as expected. The abrupt drop in L/D at 2.2° in *Figure 8c* is due to the flow transitioning to turbulnet on the upper surface which increases the drag significantly due a faster growth of thickness.

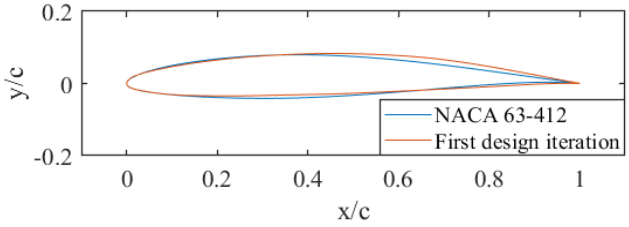

Figure 8a: Geometry of starting aerofoil and 1st-iteration

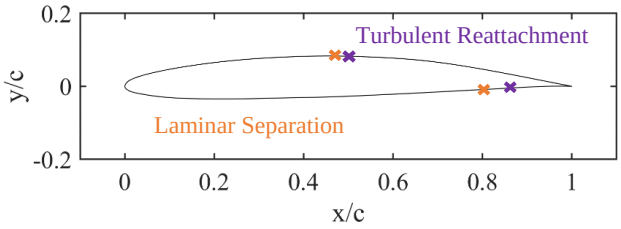

Figure 8b: 1st-iteration with critical BL points

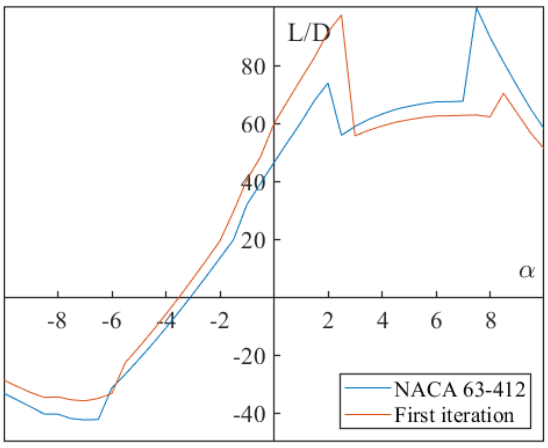

Figure 8c: Angle against lift-to-drag for 1st-iteration

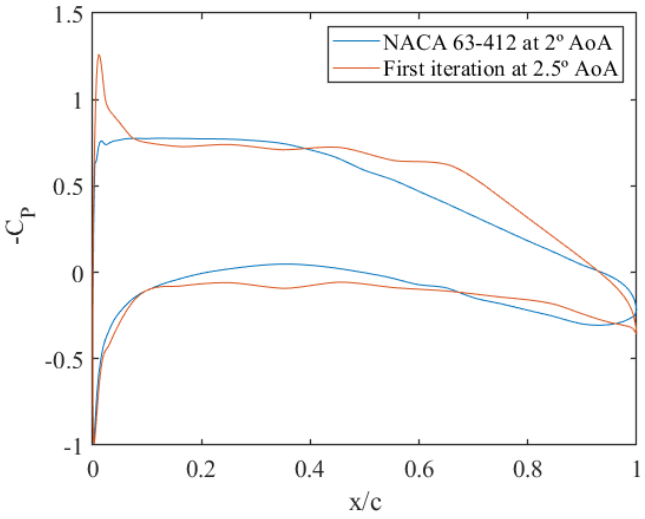

Figure 8d: Pressure distribution of starting aerofoil and 1st-iteration

Second Iteration – Delay transition

The first iteration saw a transition to turbulent on the upper surface via a separation bubble at 68% chord. Further delaying transition here is possible. In this second iteration, we attempt to reduce the adverse pressure gradient with the same method as the first iteration in order to delay transition. By just modifying the upper surface, it produced the desired change in the pressure coefficient distribution reducing the pressure gradient, but it also caused the stagnation point to move, producing a much stronger suction peak just downstream of the leading edge. As a consequence the laminar boundary layer separated immediately on the upper surface. This is undesired and so for the actual second iteration, the shape of the leading edge has been altered very subtly to try to reduce the suction peak.

Table 2: Results for first and second iteration for low-Re

			Upper				Lower	
Section	Max. L/D	α at max L/D	Laminar Separation	Turbulent Reattachment	Natural Transition	Turbulent Separation	Laminar Separation	Turbulent Reattachment
First iteration	97.42	2.5°	0.654c	0.684c	-	-	0.804c	0.840c
Second iteration	99.41	2.2°	-	-	0.746c	0.971c	0.792c	0.827c

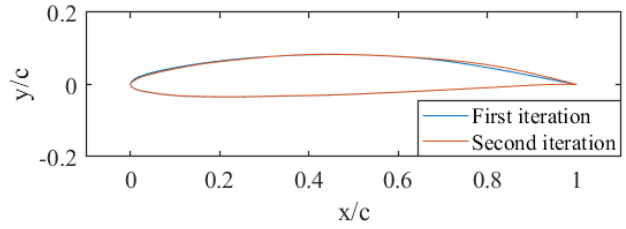

Figure 9a: Geometry of 1st and 2nd iterations

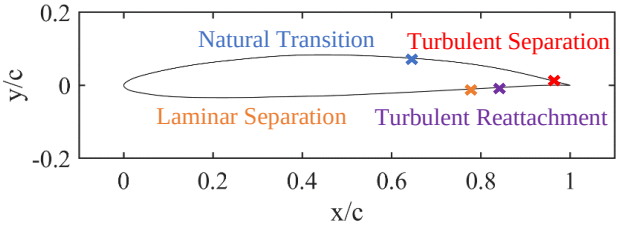

Figure 9b: 2nd iteration with BL critical points

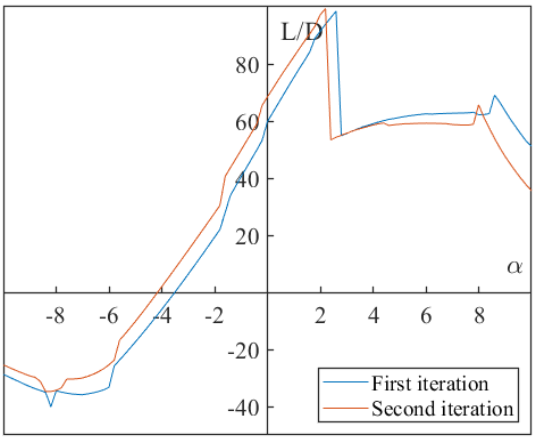

Figure 9c: Angle against lift-to-drag for 1st and 2nd iterations

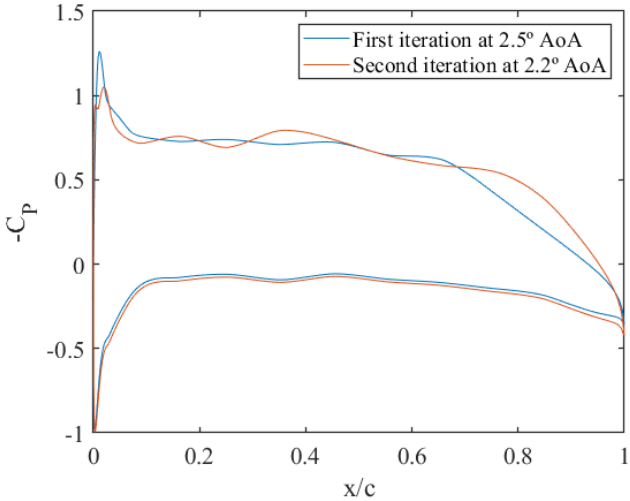

Figure 9d: Pressure distribution for 1st and 2nd iterations

The aerofoil's maximum L/D has been increased by only 2% to 99.41. However, as desired, a laminar flow is maintained on the upper surface for longer proportions of the chord length (from 68% to 75%). This iteration forms a good foundation for the final iteration.

Final design – Pressure distribution, Lift

For the final iteration, the focus will be on increasing the lift. This requires the area bounded by the upper and lower surface pressure curves to increase. We aim to achieve higher lift by adding curvature to the lower surface and modifying the nose shape to increase the strength of the suction peak. We expect the boundary layer states to change significantly and drag to increase. Although this may defeat the fine adjustments made for the first two iterations, we aim to have the increase in lift to outweigh the increase in drag.

Table 2: Results of 2nd and final iterations for low-Re

			Upper				Lower	
Section	Max. L/D	α at max L/D	Laminar Separation	Turbulent Reattachment	Natural Transition	Turbulent Separation	Laminar Separation	Turbulent Reattachment
Second iteration	99.41	2.2°	-	-	0.746c	0.971c	0.792c	0.827c
Third iteration	116.73	2.6°	0.235c	0.253c	-	1.000c	0.073c	0.090c

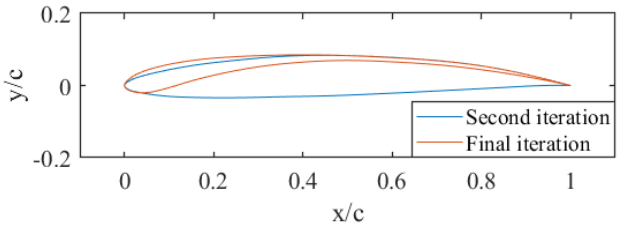

Figure 10a: Geometry of 2nd and final iterations

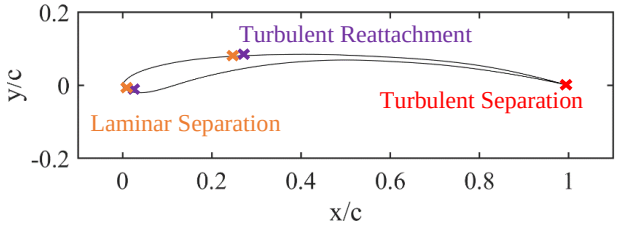

Figure 10b: 2nd iteration with BL critical points

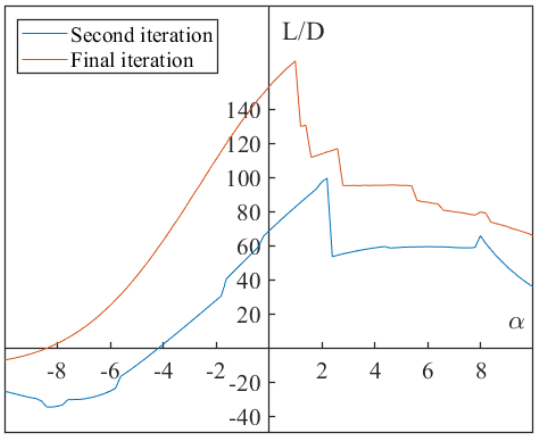

Figure 10c: Angle against lift-to-drag for 2nd and final iterations

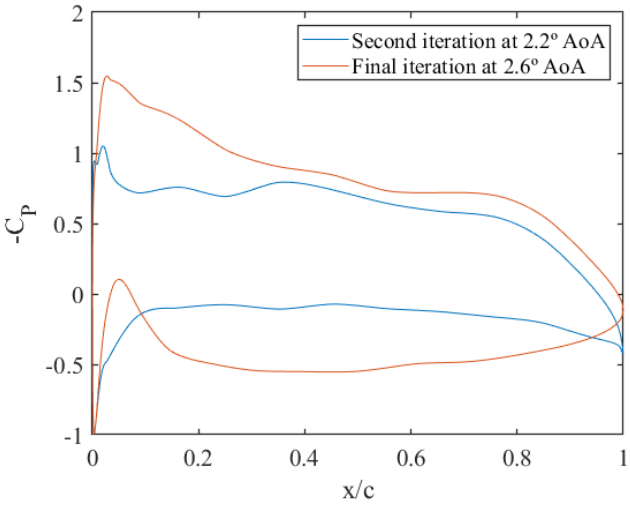

Figure 10d: Pressure distribution for 2nd and final iterations

The area bounded by the pressure curves has increased significantly in *Figure 10d* as intended, leading to a desirable 17.4% increase in L/D to 116.7. This is despite the fact that the whole of the lower surface is now turbulent, as well as an earlier transition on the upper surface.

As seen in the L/D plot in *Figure 10c*, the flow is separated at the leading edge on the lower surface at all angles of incidence below 1.6°. Although in this range of angles the maximum L/D is high, we must disregard these results as early separation means the results are invalid.

Above 1.6° the flow reattaches as a turbulent boundary layer on the lower surface and the boundary layer conditions remain similar until the angle reaches 2.8°. Here there is a drop in L/D due to an earlier transition to turbulent on the upper surface leading to higher drag. As we keep increasing the angle of attack the transition point on the upper surface will move closer to the trailing edge whereas the one on the lower surface will move towards the leading edge until we get to 8° at which the flow over the lower surface will be completely laminar. Lastly, at 12° the aerofoil stalls as the point of turbulent separation moves upstream.

This is a very advantageous feature of this design because it means it can safely operate at any angle of attack between 1.8° and 12° without stalling, with only an increase in drag when operating above the design incidence of 2.6°. Above 12° the stall is a trailing edge stall which is more gradual than an abrupt leading edge stall (separation bubble burst).

Finally, if we test the low-Re design at high-Re (20e6) and a mid-Re (10e6), we obtain the following lift over drag distribution:

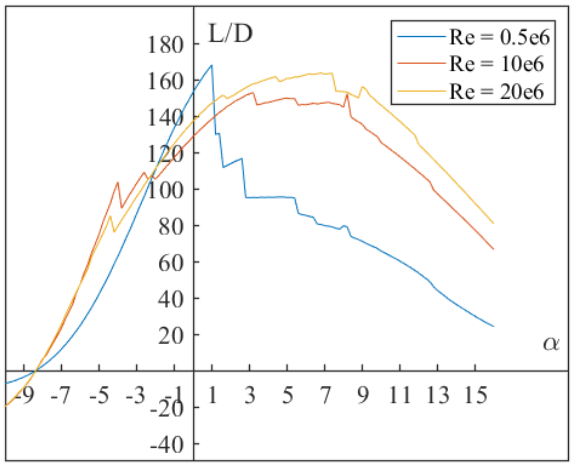

Figure 11: Lift over drag for the final design at different Reynolds numbers

There is definitely a better performance at both higher Reynolds numbers, with turbulent flow attached from -3° all the way up to 11° where turbulent separation begins to occur at the trailing edge, becoming more significant at higher angles of incidence. It even has laminar flow on the lower surface from 8° onwards which helps leads to lower drag and maintaining a high maximum L/D.

This desirable performance of the low-Re aerofoil at higher Re is very advantageous as then the aerofoil can fly at higher Re to increase the performance if needed, making the aerofoil very versatile for a range of applications.

4.2. Design Process for High Re Aerofoil (20×10^6)

The main stages in the design process are to first choose a suitable starting aerofoil which already exhibits an excellent L/D ratio. Secondly, is to increase lift and decrease drag separately, by manipulating the pressure distribution and critical boundary layer locations respectively. Lastly, is to consider the leading edge radius which affects transition to a turbulent boundary layer. [2][3] The latter can withstand a stronger adverse pressure gradient and delay separation.

Starting Aerofoil

To begin our design process for high Re aerofoil, 4 different NACA 4-digit aerofoils are considered. Sources [1][4] indicate that for a number of NACA 4-digit and 5-digit wing sections the maximum lift coefficient are the greatest for a thickness ratio of 12%. Similarly, a camber of 6% also show rapid increase of C_L [1]. Therefore NACA 0012, 6112, 6212, and 6312 sections are first analysed.

All 4 aerofoils show a similar trend of increasing life-to-drag ratio (L/D) with increasing angle of attack up until the point of stall (significant turbulent separation on the upper surface) as seen in *Figure 12a*. 6312, 6212, and 6112 all have comparable maximum L/D ratios and all 3's L/D ratios drop abruptly as their locations of turbulent separation move upstream, leading to an increase in wake form drag. 0012 has much lower L/D throughout due to lower lift from a lack of camber. Unlike the low-Re laminar aerofoil, there is a lesser presence of a 'laminar bucket' as seen in *Figure 12b*. This implies at higher Re, the optimum range of incidence (minimum C_D is achieved at a range of C_L) is smaller and the aerofoil less flexible.

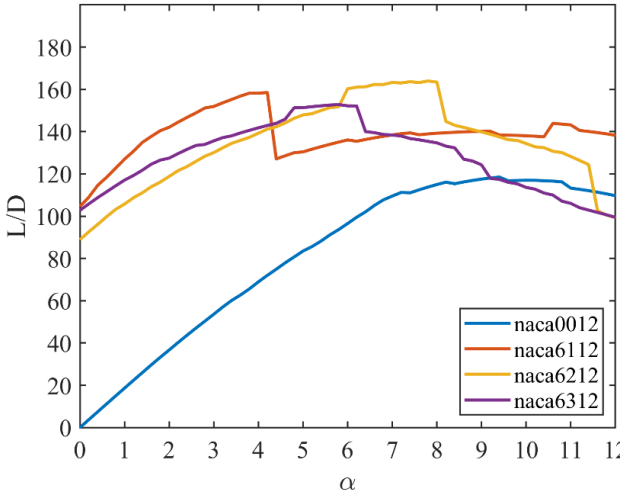

Figure 12a: Angle against lift-to-drag ratios for naca aerofoils

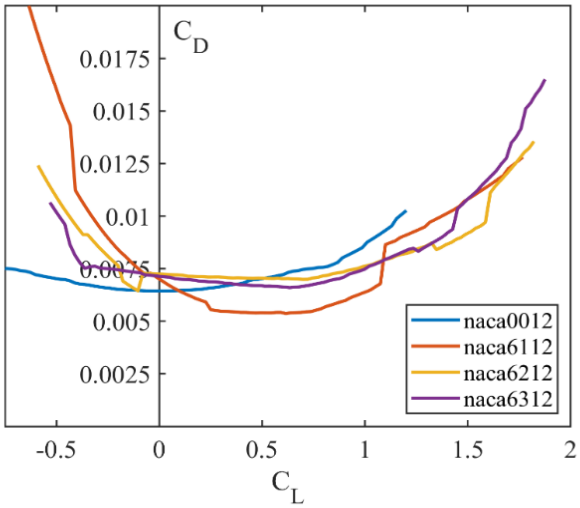

Figure 12b: Lift against drag for naca aerofoils

NACA-6212 is chosen as our starting aerofoil due to it exhibiting the highest maximum L/D of 163.4 at 8°. Although *Figure 12b* shows that NACA-6112 has a relatively lower drag curve to 6212, 6212 has a higher overall L/D at higher incidences where lift is maximum. There is definitely room for improvement as there is a lack of curvature on the lower surface hence pressure could be increased there, but also the fact that at this 8° incidence, there is natural transition on the lower surface at $x = 0.611c$. Similar to low-Re aerofoil, by delaying transition, drag could be reduced as a laminar boundary layer exhibits a slower growth.

First iteration – Pressure, Lift

The first design iteration's main aim is to increase the C_L, by increasing and reducing the pressures on the lower surface and upper surface respectively. On a graph of coefficient of pressure against aerofoil x-location, the aim is to increase the area bounded by the upper and lower surface curves. Note that boundary layer states and drag reduction is not considered here.

Table 3: Results of starting aerofoil and first iteration for high-Re

			Upper		Lower
Section	Max. L/D	α at max L/D	Natural Transition	Turbulent Separation	Natural Transition
NACA-6212	163.4	8°	0.126c	0.993c	0.611c
First iteration	184.3	7.6°	0.126c	1.000c	0.320c

NACA-6212's upper surface already has a considerable amount of curvature. Different upper surface curvature modifications were tested, these included: increasing curvature by both increasing suction peak height or average height, and altering the location of the suction peak or maximum thickness. All trials led to no significant increase in maximum L/D and in most cases led to a reduction in the maximum L/D. Therefore, for this iteration the focus was shifted towards the lower surface.

One way to shift the upper surface pressure curve in *Figure 13d* to a lower pressure without significant alterations to the upper surface geometry, is to shift the location of the leading edge stagnation point towards the upper surface. This was done by increasing the gradient just past the leading edge on the lower surface.

We require the lower surface's pressure to increase to increase the overall lift, this was done by increasing the curvature which essentially increases the camber. As can be seen from the pressure plot in *Figure 13d*, although the pressure near the leading edge has been reduced by a small amount, the pressure for the rest of the lower surface has been increased significantly. This rise in lower surface pressure alters the angle at which maximum L/D occurs, alongside the fact that the leading edge stagnation point has now moved upwards, the upper surface now sees a reduction in pressure.

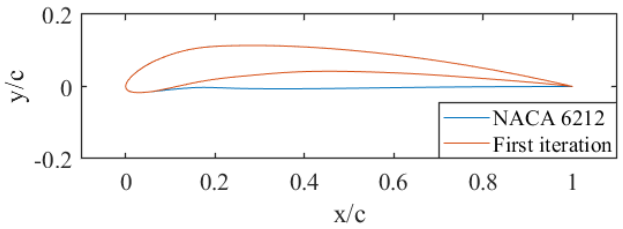

Figure 13a: Geometry of naca6212 and 1st iteration

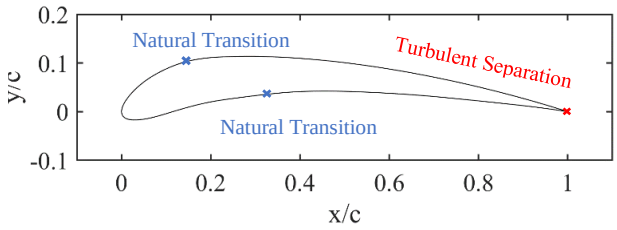

Figure 13b: 1st iteration and critical BL points

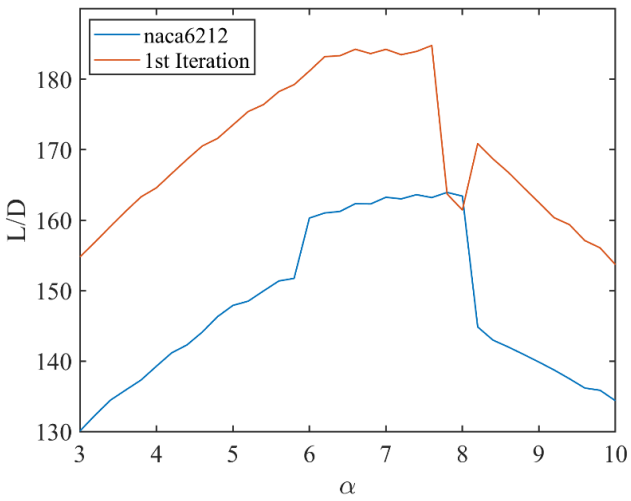

Figure 13c: Angle against lift-to-drag ratio comparison

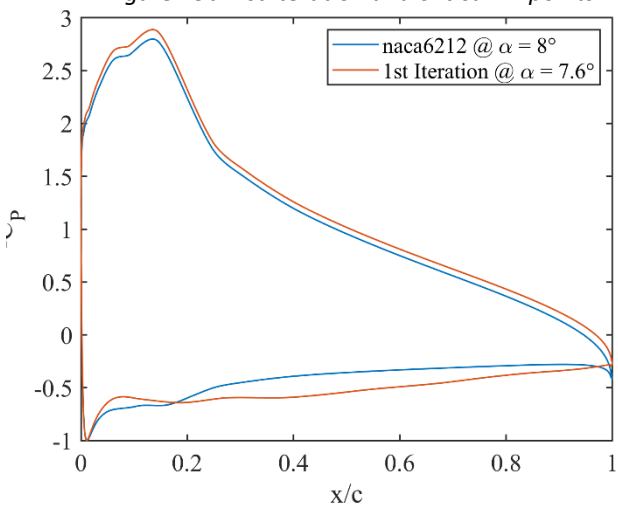

Figure 13d: Pressure distribution comparison

The maximum L/D ration has been increased by 13% to 184.8. Similar to the starting aerofoil, the first iteration design's L/D drops suddenly past 7.6° due to an earlier turbulent separation. However, since the focus of this iteration was not on the drag, we can see ways in this could be improved. For instance, at the optimum angle, natural transition on the lower surface occurs at $x = 0.32c$. This could be delayed, leading to a slower boundary layer growth for while it is laminar for longer.

Second iteration – Pressure, Lift

Before moving on to manipulate the location of boundary layer natural transition, we should attempt to further increase the curvature mainly on the lower surface and slightly on the upper surface similar to the first iteration. This led to a massive 10.3% increase in L/D ratio to 203.8. However, this is invalid because for all angles of incidence below 5°, the turbulent boundary layer separates at the leading edge ($x = 0.153c\ for\ 5°$) on the lower surface. This is due to a sharp curvature just behind the stagnation point. On the pressure plot in *Figure 14d*, this corresponds to a strong adverse pressure gradient between $x = 0.05c\ to\ 0.15c$, leading to separation.

Table 4: Results of first and second iteration for high-Re

			Upper	Lower	
Section	Max. L/D	α at max L/D	Natural Transition	Natural Transition	Turbulent Separation
First iteration	184.3	7.6°	0.126c	0.320c	N/A
Second iteration	203.8	5.0°	0.138c	0.063c	0.153c

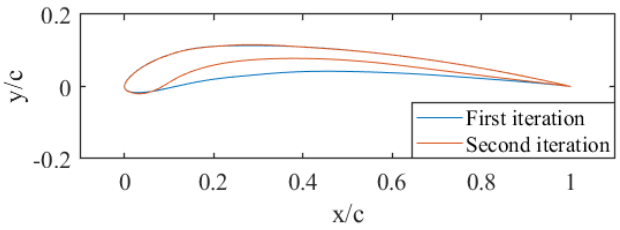

Figure 14a: Geometry of 1st and 2nd -iteration

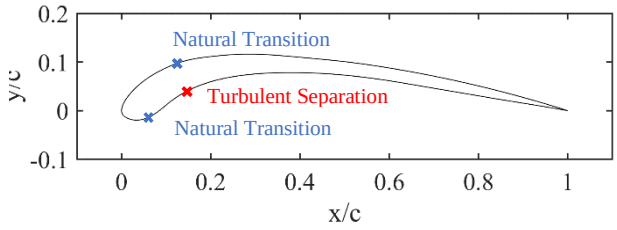

Figure 14b: 2nd-iteration with critical BL state points

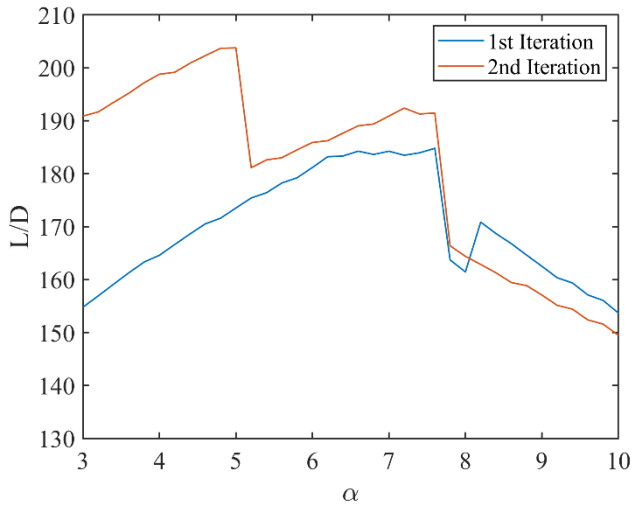

Figure 14c: Angle against lift-to-drag ratio comparison

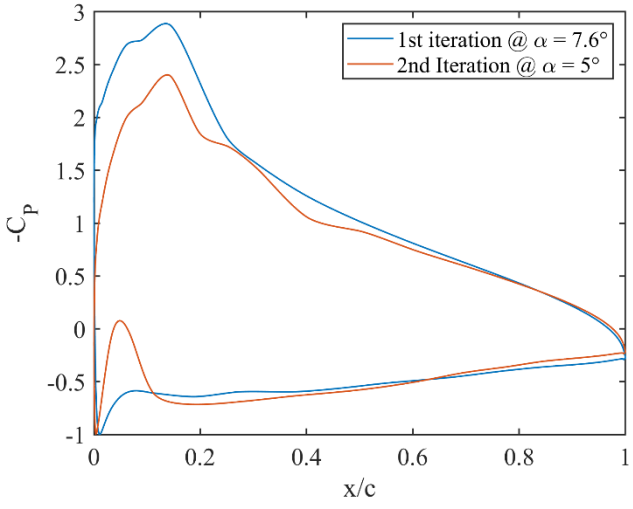

Figure 14d: Pressure distribution comparison

This early separation means the results are invalid, because our code for the lift does not take into account separation, whereas in practice there would be a massive reduction in lift at stall/early separation. Fascinatingly, the flow does not separate at angles greater than 5°, and between 5° and 7.6° the L/D ratio is still higher than the first iteration.

This iteration was a worthwhile discovery. It has shown that by further increasing the lower surface curvature the pressure could be increased even further as expected, leading to higher maximum L/D. Although invalid due to early separation, if the pressure peak behind the leading edge on the lower surface is to be made more gradual, by smoothening the geometry in the next iteration, then turbulent separation and even natural transition could be delayed (lower drag) while maintaining the phenomenally high lift achieved here.

Third and Final Iteration – Boundary Layer, Drag

As mentioned earlier, we aim to avoid turbulent separation around the leading edge on the lower surface as that is an invalid non-realistic aerofoil. Similarly, we also need to delay natural transition on both surfaces, as that would lead to lower drag due to laminar boundary layers exhibiting slower thickness growths. This was both achieved in the third iteration by sharpening the nose of the aerofoil, which meant the curvature immediately behind the leading edge on the lower surface is more gradual.

Table 5: Results of third iteration for high-Re

			Upper	Lower	
Section	Max. L/D	α at max L/D	Natural Transition	Natural Transition	Turbulent Separation
Second iteration	203.8	5.0°	0.138c	0.063c	0.153c
Third iteration	211.4	7.2°	0.129c	0.997c	N/A
Final iteration	210.1	7.2°	0.127c	0.997c	1.000

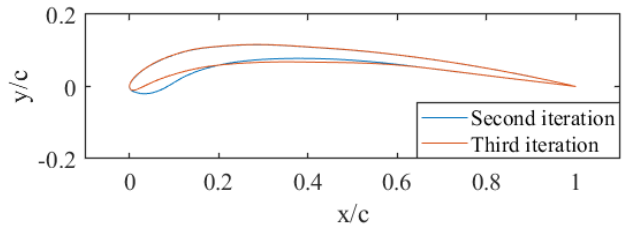

Figure 15a: Geometry of 2nd and 3rd iterations

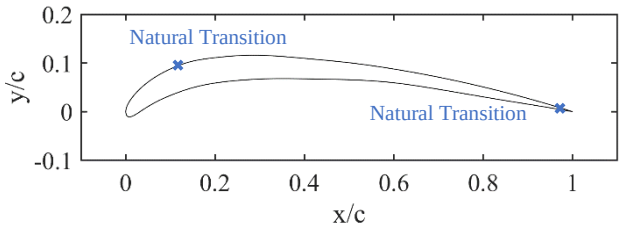

Figure 15b: 3rd-iteration with critical BL state points

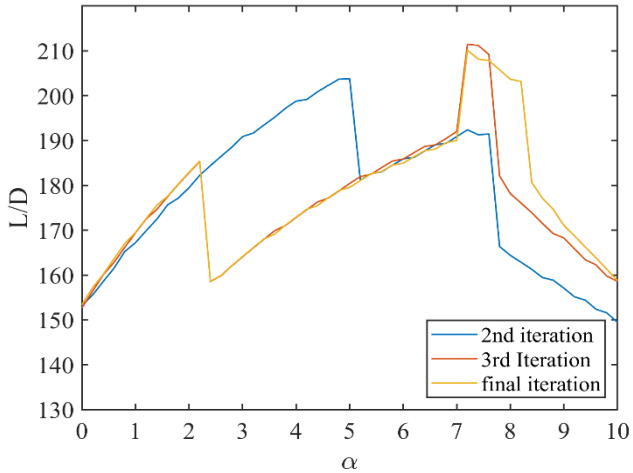

Figure 15c: Angle against lift-to-drag ratio comparison

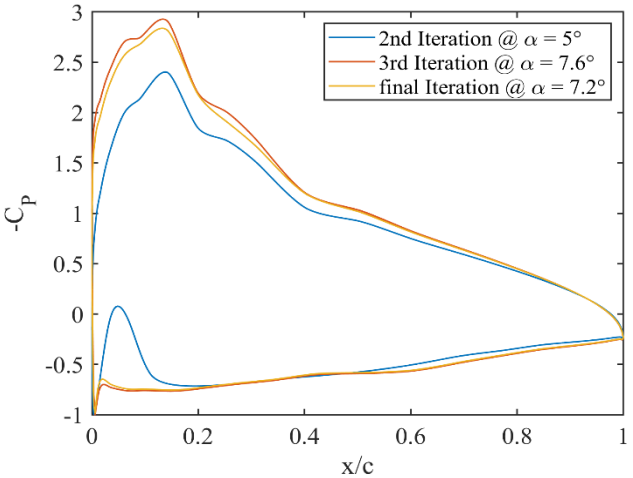

Figure 15d: Pressure distribution comparison

This new lower surface curvature meant the flow not only stays attached at lower angles of incidence, but also as we intended stays laminar on the lower surface throughout at the optimum angle, leading to a drop in drag. This led to a massive 14.7% gain in L/D from 184.3 (using 1st iteration because 2nd iteration is invalid due to early separation) to 211.4 as expected. The pressure plot (*Figure 15d*) shows that at 7.2° the strong adverse pressure gradient on the lower surface has now disappeared.

For the third iteration, leading edge turbulent separation on the lower surface now occurs at a much lower 2.2° instead of 5°. This means from 2.3° to 7.2°, even though the L/D ratio is not at the aerofoil's maximum designed value, the aerofoil is still usable, ranging from L/D = 160-190; an improvement from the second iteration. This lower L/D from 2.3° to 7.2° is due to the fact that natural transition to turbulent occurs at the leading edge instead of the trailing edge, leading to a higher drag. However, as can be seen in *Figure 15c*, the range of optimum L/D for the third iteration only occurs between 7.2° to 7.6°. Past 7.6° there is significant turbulent separation on the upper surface. This 0.4° range of operation is not ideal, so the aim for the final iteration is to improve the range of angles which the optimum L/D ratio is achieved.

For the final optimum design, fine modifications to a few selections of geometry nodes were done, especially around the leading edge, where the boundary layer's reaction to a change in angle of incidence is more sensitive. The aim to extend the optimum angles was achieved, as seen in *Figure 15c*, a high L/D ratio was maintained until 8.2°, so the range is now 1°. This means if operating at the maximum L/D at 7.2°, the angle of attack could fluctuate more before turbulent separation on the upper surface and hence stall is observed. However, the pressure magnitude on the upper surface has been reduced, leading to slightly lower maximum L/D of 210.1 (and L/D is 203.1 at angle of 8.2°). We conclude that however, the benefits of flexibility in angle of incidence outweigh the benefits of a marginally higher L/D ratio.

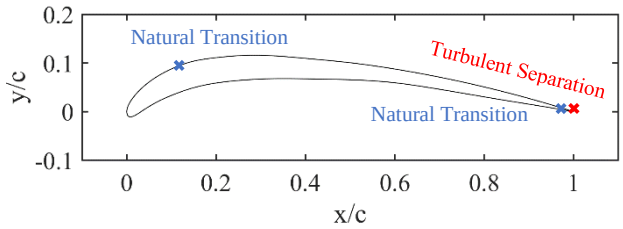

Figure 16: Geometry of final-design with BL state locations

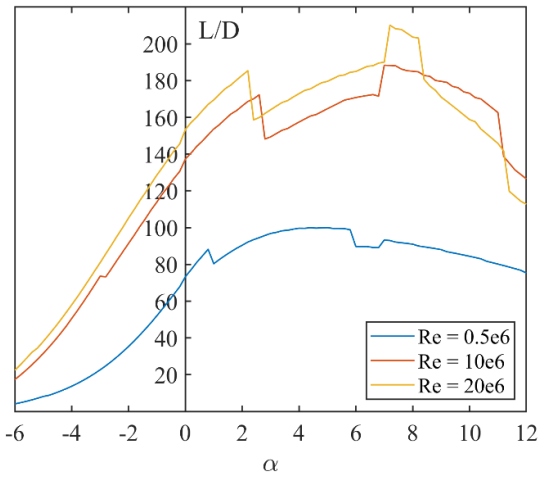

Figure 17: High-Re design's angle against lift-to-drag ratio at different Re

The final design for high Re (20e6) has also been tested at low Re (0.5e6) and a mid Re (10e6). Results are plotted in Figure 12. The mid-Re curve has a similar shape to high Re, albeit shifted downwards. This indicates that the boundary layer performance is similar: leading edge (LE) turbulent separation on the lower surface angles smaller than 2°, LE transition to turbulent on the lower surface up to 7°, and fully laminar lower surface above 7°. The only difference is that for mid-Re, significant upper surface turbulent separation does not happen until 11°, this means the range of high L/D is maintained until much later. For low-Re however, this aerofoil design

is very inefficient. There is LE turbulent separation on the lower surface at angles smaller than 5.8°, and LE transition on the lower surface between 5.8° and 6.6°. The maximum L/D is 99.98, but this is at 5° and hence invalid due to early separation. The highest valid L/D is then 93.27 at 7°.

6. Reliability of Results

There are two assumptions in our Matlab model. One assumption was made which says skin friction drag is negligible relative to form drag and hence was not considered in our model. Although a turbulent boundary layer has higher skin friction drag than a laminar boundary layer, the majority of drag contributions are from pressure form drag, so the drag coefficient was purely calculated with the boundary layer condition at the trailing edge (aerofoil wake). The second assumption is that the boundary layer remains thin throughout. This is important because our lift calculation uses the inviscid solution and assumes no boundary layers. This was checked: the displacement thickness at the trailing edge of the high-Re final design is $\delta^*/L = 0.00017$. These values clearly small enough to suggest this assumption is valid.

As mentioned in the aerofoil validation section, our Matlab model is unreliable when the aerofoil is stalled, or equivalently when turbulent separation occurs on the upper surface. Rather than a rapid increase in drag and dop in lift as one would expect from real-life observations, our model continues to predict a high L/D ratio. Therefore, when looking at results for each design iteration, great care was taken to not purely analyse the L/D plots, but also the location on both surfaces where separation (if any) occurs. If separation occurs significantly far away from the trailing edge, the results were said to be invalid, and better designs were considered to mitigate these early separations. Our final iterations have turbulent separation occurring at $x = 1.000$ for both low-Re and high-Re, indicating reliable results at their optimum operating points.

Another feature which our model cannot predict accurately is the separation bubble, which is the region between laminar separation and turbulent reattachment. Our model treats this region the same as an attached turbulent boundary layer. However, a separation bubble effectively increases camber, causing a change in air pressure, and thus affects the lift and drag. [6] On a pressure coefficient plot, the separation bubble region should be a flat line, indicating a constant C_P characteristic [6]. For our low-Re design, a separation occurs for all iterations on both upper and lower surfaces. The size of the bubble for the final design has length 0.017c, indicating that the bubble is in fact negligible and results are still relatively reliable.

Lastly, F.W. Schmitz observed that there are 2 values of critical Re (separation occurring instead of transition), it is higher when increasing Re (subcritical to supercritical) and lower when decreasing Re. This is known as hysteresis. [6] Our model only has one value of critical Re. However, this has little effect on our results' reliability as we tested each aerofoil design at one fixed Re.

7. Conclusion

A Matlab numerical model was developed by combining the inviscid solution with the boundary layer solution. This allowed any aerofoil sections to be analysed to give performance

metrics such as lift and drag, as well as boundary layer conditions, at different angles of incidence. 2 aerofoil sections were designed for low-Re and high-Re, by manipulating the pressure distributions and critical boundary layer state locations through several iterations. L/D was determined the most important parameter, but stall characteristics and range of operation were also considered, with our high-Re final design sacrificing some L/D for extra range of optimum operating angles. Our numerical model used several underlying assumptions about physical processes which reduced the accuracy of our results but some were shown to have negligible effects. In conclusion:

- A resolution of 400-panels in our panel method was sufficiently accurate to model the lift and drag characteristics of an aerofoil. 500-panels was used for the majority of the design process while 800-panels was used for the final iterations.
- Our model was validated with experimental data for NACA 0012 and 4412 sections and found to agree within a few percent until the point of separation.
- An optimal aerofoil for $Re = 0.5 \times 10^6$ achieved a maximum L/D of 116.73
- An optimal aerofoil for $Re = 20 \times 10^6$ achieved a maximum L/D of 210.1

8. References

[1] Chapter 7, Abbott & von Doenhoff 'Theory of Wing Sections', Dover

[2] Chapters 7–9, Simons, 'Model aircraft aerodynamics', Argus Books

[3] Chapter 2, Hoerner, 'Fluid dynamic drag', Hoerner Fluid Dynamics

[4] Chapter 2, Hoerner, 'Fluid dynamic lift', Hoerner Fluid Dynamics

[5] Airfoil database search (NACA 6 series), Airfoil Tools, http://airfoiltools.com/search/index?m%5Bgrp%5D=naca6&m%5Bsort%5D=1, (accessed on 01/06/21)

9. Appendix

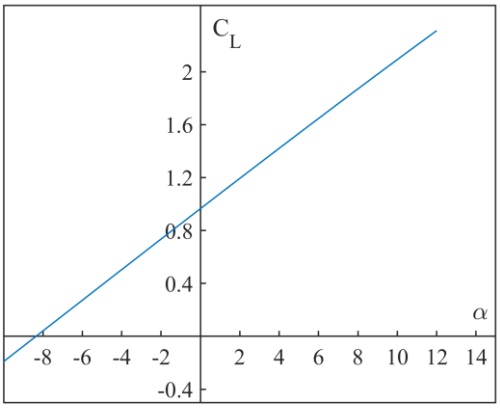

Figure 18a: Angle against lift coefficient for the final low-Re design

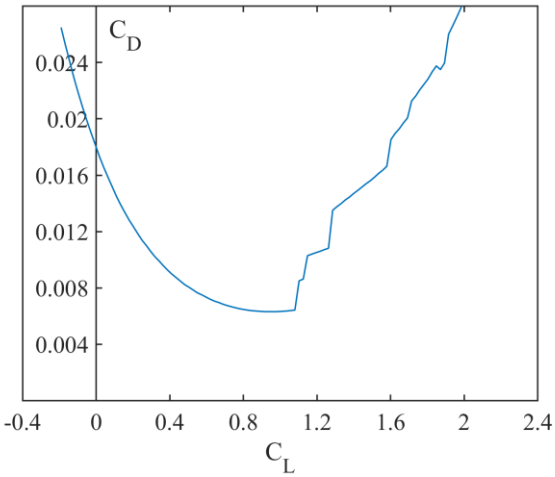

Figure 18b: Coefficient of lift against drag for the final low-Re

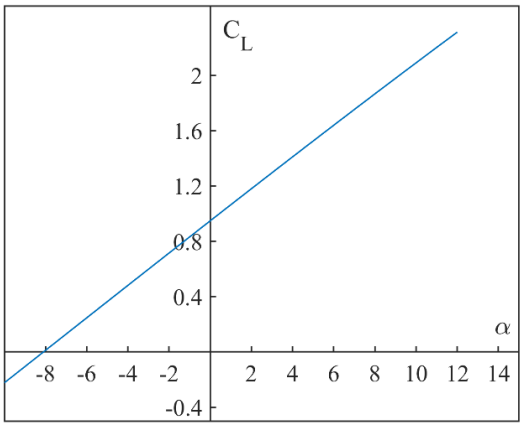

Figure 19a: Angle against lift coefficient for the final high-Re design

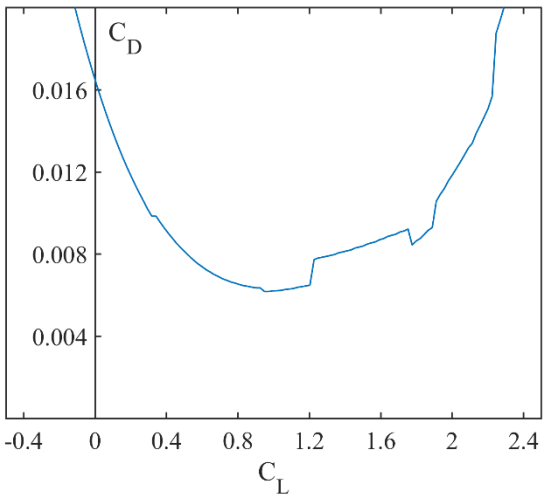

Figure 19b: Coefficient of lift against drag for the final high-Re design

Table 7: Low-Re final design .surf file

1.0000000e+00	0.0000000e+00
9.3027888e-01	2.1912351e-02
8.5537849e-01	4.2629482e-02
7.6852590e-01	6.0159363e-02
6.6494024e-01	7.2908367e-02
5.5577689e-01	8.0876494e-02
4.5477530e-01	8.5563745e-02
3.4860558e-01	8.5657371e-02
2.5219124e-01	8.1673307e-02
1.6294821e-01	7.2908367e-02
8.9641434e-02	5.7768924e-02
3.3864542e-02	3.7051793e-02
7.5697211e-03	1.7131474e-02
0.0000000e+00	0.0000000e+00
6.6400000e-03	-8.7100000e-03
2.7430000e-02	-1.7160000e-02
8.7250996e-02	-8.3665339e-03
1.4382470e-01	1.2350598e-02
2.2270916e-01	3.6254980e-02
3.0717131e-01	5.4581673e-02
3.8605578e-01	6.4940239e-02
5.0000000e-01	7.0517928e-02
6.1075697e-01	6.5737052e-02
7.0478088e-01	5.7768924e-02
8.2270916e-01	4.0239044e-02
9.3984064e-01	1.5537849e-02
1.0000000e+00	0.0000000e+00

Table 6: High-Re design .surf file

1.0000000e+00	0.0000000e+00
9.5098000e-01	1.4236000e-02
9.0171400e-01	2.7605000e-02
8.0287500e-01	5.1804000e-02
7.0339200e-01	7.2740000e-02
6.0340100e-01	9.0343000e-02
5.0296900e-01	1.0434100e-01
4.0217300e-01	1.1420700e-01
3.1240600e-01	1.2055300e-01
2.5055700e-01	1.2067100e-01
1.9798400e-01	1.1733800e-01
1.4207100e-01	1.0911000e-01
8.9611000e-02	9.1093000e-02
6.0253000e-02	7.5887000e-02
3.5413000e-02	5.8666000e-02
1.3176000e-02	3.7384000e-02
3.0040000e-03	2.3237000e-02
-6.7000000e-04	1.5096000e-02
-1.8340000e-03	9.9980000e-03
-1.9720000e-03	6.7270000e-03
0.0000000e+00	0.0000000e+00
3.0726257e-02	7.9808460e-03
9.0582602e-02	3.7509976e-02
1.4804469e-01	5.5865922e-02
2.1428571e-01	6.7039106e-02
2.7494014e-01	7.1635275e-02
3.4357542e-01	7.3231445e-02
4.1620112e-01	7.1827614e-02
5.0478851e-01	6.9433360e-02
6.0295291e-01	6.2250599e-02
6.9313647e-01	4.9481245e-02
7.7294493e-01	3.6509976e-02
8.4536872e-01	2.4740623e-02
9.0603459e-01	1.5274336e-02
1.0000000e+00	0.0000000e+00